ACS APPLIED MATERIALS & INTERFACES

Research Article

www.acsami.org

Preparation of Yellowish-Red Al-Substituted α-Fe_2O_3 Powders and Their Thermostability in Color

Hideki Hashimoto,*[,†] Makoto Nakanishi,[†] Hiroshi Asaoka,[†] Tomoaki Maeda,[†] Yoshihiro Kusano,[‡] Tatsuo Fujii,[†] and Jun Takada[†,§]

[†]Graduate School of Natural Science and Technology, Okayama University, Okayama 700-8530, Japan

[‡]Department of Fine and Applied Arts, Kurashiki University of Science and the Arts, Kurashiki, Okayama 712-8508, Japan

[§]JST, CREST, Okayama 700-8530, Japan

Supporting Information

ABSTRACT: Inspired by the traditional Japanese pigment Fukiya bengala, nanocomposite materials were synthesized using a polymer complex method, comprising Al-substituted α-Fe_2O_3 (hematite) particles with diameters ranging from 40 to 100 nm and ultrafine Fe-substituted α-Al_2O_3 (corundum) particles smaller than 10 nm in diameter. The obtained powders exhibited a vivid yellowish-red color and high thermostability, making them attractive as potential overglaze enamels on porcelain. Quantitative color measurements revealed that, when heated to 700, 800, and 900 °C, samples displayed high lightness (L^*) and color-opponent dimensions (a^* and b^*) at 10 mol % Al. For the same particle size samples, L^*, a^*, and b^* values increased with the Al molar ratio, revealing that Al substitution in the hematite structure intrinsically enhances lightness and chroma in hematite color. These samples mostly retained their color upon reheating at 900 °C, indicating their high thermostability. This thermostability should originate from the Al substitution-induced enhancement in lightness and chroma in hematite color, which should counter color fading caused by particle growth. These composite materials are expected to find application in the porcelain industry, cosmetics, and nanotechnology.

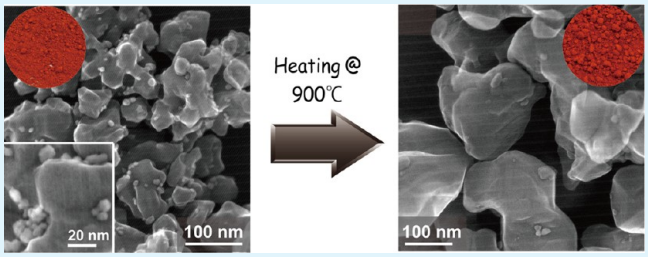

KEYWORDS: *iron oxides, hematite, aluminum, color, thermostability*

INTRODUCTION

Hematite has recently become an important material in nanotechnology because of its potential use as a catalyst, gas sensing material, electrode material for lithium-ion batteries, and photoanode material for photoelectrochemical water splitting.[1−8] Various methods have been developed to precisely control hematite particle size, distribution, dispersibility, and morphology and optimize their performance for these applications.[1−11]

Hematite has widely been used as a red pigment since the prehistoric times.[12−14] Hematite-based red pigments, bengala in Japan, are commonly used as pigments for overglaze enamels of porcelain, lacquer wares, asphalt roads, cosmetics, and building materials[12−14] because of their excellent tinting strength and weather resistance. Hematite powders displaying a beautiful red color are often applied on porcelain bodies.[15−25] In this paper, "beautiful red color of hematite powders" means that the color shows high L^*, a^*, and b^* values in the CIE1976 $L^*a^*b^*$ color space.[26] When used to color porcelain bodies, hematite is blended with appropriate glazes and solvents to form a mixture that is applied on the porcelain, which is subsequently heated to high temperatures between 700 and 900 °C.[15] In general, the color of hematite powders depends on particle size. Lightness and chroma increase with decreasing particle size, while color fades with heat-induced grain growth at high temperatures.[14,27,28] Therefore, highly thermostable hematite powders, which do not fade in color when heated to high temperatures, are strongly needed in the porcelain industry. Chemical stability in molten glazes is also a key factor. The downsizing of pigment particles in the range of wavelength of light increases the chromaticity; however, such small particles are easily dissolved in glazes.[13,29−31] Recently, chemically stable inclusion pigments have attracted considerable research interest.[18−25] These pigments combine colored crystals and an uncolored phase displaying good chemical and thermal stabilities, such as hematite and amorphous silica, resulting in excellent stabilities.

Here, hematite powders exhibiting beautiful color and high thermostability were prepared using an unconventional approach. This work was inspired by Fukiya bengala, the first artificial bengala produced in Japan.[12,32,33] Fukiya bengala was manufactured from 1707 to 1970 in the small village of Bichu-Fukiya-Mura in the northern part of Okayama prefecture. Because of its high-quality red color, it was used by potters throughout Japan for Kutani and Arita wares, and in addition,

Received: August 28, 2014
Accepted: October 14, 2014
Published: October 14, 2014

its precursor Fukiya melanterite ($FeSO_4 \cdot 7H_2O$) was used for Arita ware. These facts are indicative of the magnificence of Fukiya bengala.[34−36] At that time, porcelains decorated with beautiful aka-e red patterns, known as Kakiemon-style ware, were extremely attractive and impressive. Exported to Europe and the United States from the later 17th century, Kakiemon-style ware presents a simple colorful design on a sufficient white milky space that enthralled royalty and aristocrats and continues to be revered by admirers worldwide.[36−40] The manufacturing of Fukiya bengala was prohibited by an antipollution law in 1970 because it emitted numerous sulfur oxides and water-soluble sulfates, causing the disappearance of this pigment. However, renowned potters in Japan are still longing to use Fukiya bengala for their artistic red overglaze enamels.

In a detailed investigation of existing Fukiya bengala, we showed that its main component consisted of hematite fine particles incorporating 1 mol % Al.[33] We also synthesized Al-substituted hematite powders to assess the role of Al, and indicated that Al substitution suppressed hematite particle growth, leading to enhance hematite color.[33,41] However, the relation between hematite color and Al content, microstructures, and thermostability of the powders remains unclear because the work on synthetic Al-substituted hematite is very preliminary. Here, Al-substituted hematite powders were synthesized and their color properties, microstructures, and thermostability were investigated in detail.

EXPERIMENTAL SECTION

On the basis of our previous report, Al-substituted hematite samples were synthesized by the polymer complex method.[41] The experimental conditions were slightly modified. Samples contaiting Al molar ratios [x = Al/(Fe + Al)] ranging from 0 to 0.30 in 0.05 increments were prepared. Reagents used in this study were $Fe(NO_3)_3 \cdot 9H_2O$ (Nakalai Tesque, 99%), $Al(NO_3)_3 \cdot 9H_2O$ (Nakalai Tesque, 99%), citric acid (Wako Pure Chemical Industries, 98%), and ethylene glycol (Tokyo Chemical Industry, 99.5%). The mixture of (Fe + Al):(citric acid):(ethylene glycol):(distilled water) = 1:5:15:50 molar ratio was heated at ∼80 °C for 7 h to form metal−citrate complexes and subsequently at 170 °C for 12 h in air. The obtained solids were pyrolyzed at 445 °C for 24 h in air to remove organic components. Heating conditions are summarized in Table S1 in the Supporting Information.

The obtained pyrolytic powders were ground, pressed into pellets, heated at temperatures ranging from 500 to 1100 °C in 50 °C increments for 2 h in air, except for 1050 °C, and quenched to room temperature (see Figure S1 in the Supporting Information). Hereafter, the heated samples with different Al contents will be noted as (temperature value)-(100 × x). For example, 700-10 corresponds to a sample with an x value of 0.10 heated at 700 °C. To clarify the effects of heat treatment on color tone, some heated samples were reheated at 900 °C for 1 h.

Constituent phases were determined by powder X-ray diffraction (RINT-2500, Rigaku) using a monochromatic Cu−Kα radiation. Lattice parameters of heat-treated samples were refined from XRD profiles using silicon as an internal standard (NIST SRM660d). Formation processes under air flow were characterized using a thermogravimetry-differential thermal analysis (TG-DTA) apparatus (TG8120, Rigaku). Color tone and reflection spectra were measured by spectrophotometry (CM-2600d, Konica Minolta Sensing) using CIE Standard Illuminant D_{65}. A commercially available hematite (Kojundo Chemical Lab. Co., Ltd.; Purity: 99.99%) and Fukiya bengala were also measured by spectrophotometry. For reflection spectra measurements, powder samples were pressed into a glass holder (ϕ = 8 mm) using a glass plate to flatten the compacted powders' surface. The microstructure was examined by scanning electron microscopy (SEM) (JED-2200F, JEOL) and transmission electron microscopy (TEM) (JEM-2100F, JEOL) coupled with secondary electron (SE) detection, and energy-dispersive X-ray spectrometry (EDS). High-resolution TEM (HRTEM) images were acquired in TEM mode while SE and EDS elemental mapping images were acquired in scanning TEM (STEM) mode with a CEOS C_s corrector (for spherical aberration correction for condenser lens).

RESULTS AND DISCUSSION

Constituent Phases and Solubility Limits of Al. XRD patterns of the pyrolytic powders and heat-treated samples are shown in Figures 1 and 2, respectively. The diffraction peaks

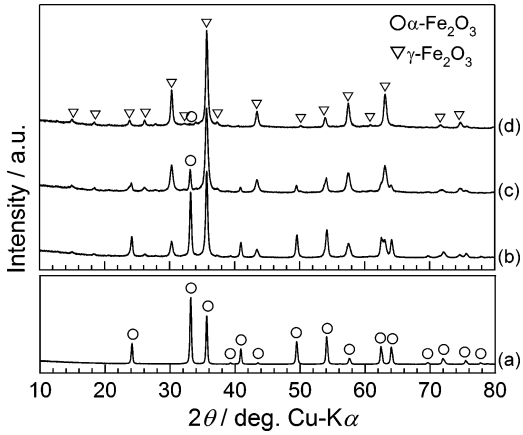

Figure 1. XRD patterns of pyrolytic powders at different Al molar ratios (a) x = 0, (b) 0.05, (c) 0.15, and (d) 0.30.

were assigned by using powder diffraction files of the ICDD database, PDF 00-039-1346, 00-033-0664, 00-030-0024, and 00-046-1212 for hematite, γ-Fe_2O_3 (maghemite), $AlFeO_3$, and α-Al_2O_3 (corundum), respectively. The XRD patterns revealed that hematite formed in Al-free and Al-containing samples and maghemite also existed in Al-containing pyrolytic samples. The Al-free pyrolytic sample was monophasic hematite. For $x \geq$ 0.05, the pyrolytic samples comprised Al-substituted hematite (Al-Hem) and Al-substituted maghemite (Al-Mag), and the Al-Mag peak intensity increased with increasing Al molar ratio (Figure 1). After heat treatment, the constituent phases changed depending on the Al molar ratio and temperature. Hematite formed in all heat-treated samples, while the other phases exhibited peak intensities that increased with increasing Al molar ratio. For $x \geq$ 0.05, samples heated at 500 °C contained Al-Mag (Figure 2a). For $x \geq$ 0.15, samples treated at 650 °C consisted of Al-Mag and $AlFeO_3$, (Figure 2b) and those heated at 800 °C comprised $AlFeO_3$ (Figure 2c). Samples heated at 900 °C contained Fe-substituted corundum (Fe-Cor) for x = 0.15 but were composed of $AlFeO_3$ and Fe-Cor for $x \geq$ 0.20 (Figure 2d). For $x \geq$ 0.15, samples treated at 1100 °C contained Fe-Cor (Figure 2e). The constituent phases with different temperatures and Al molar ratios are summarized in Figure 2f. Al-Hem was obtained as a single phase at high temperature ($T \geq$ 700 °C) and low Al molar ratio ($x <$ 0.15). At higher Al molar ratio ($x \geq$ 0.2), constituent phases gradually changed from (Al-Hem + Al-Mag) to (Al-Hem + Al-Mag + $AlFeO_3$), (Al-Hem + $AlFeO_3$), (Al-Hem + $AlFeO_3$ + Fe-Cor), and (Al-Hem + Fe-Cor) with increasing heat-treatment temperature. These results suggest that Al-Mag and $AlFeO_3$ decompose into (Al-Hem + $AlFeO_3$) and (Al-Hem + Fe-Cor), respectively. In the present study, the coexistence region of three phases, (Al-Hem + Al-Mag + $AlFeO_3$), appeared and the

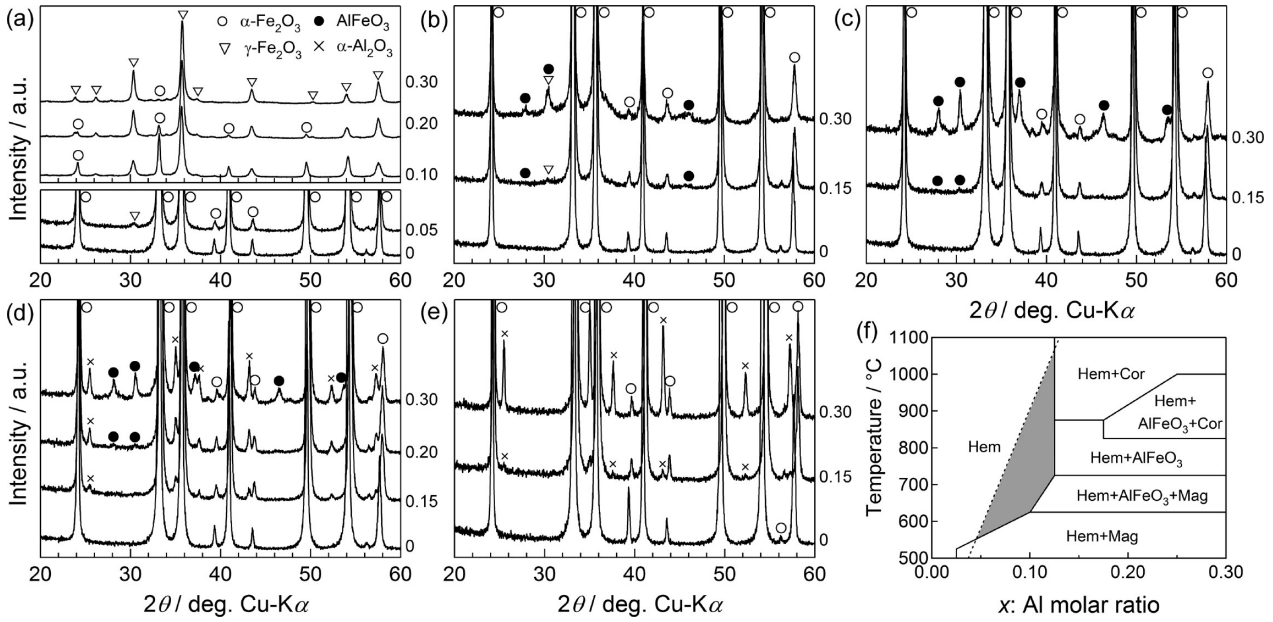

Figure 2. XRD patterns of heat-treated samples. (a–e) Samples heated at 500, 650, 800, 900, and 1100 °C, respectively. Al molar ratios (x) are shown beside the corresponding patterns. (f) Constituent phase diagram of heat-treated samples. The dotted line in the diagram shows solubility limit of Al in the hematite structure determined from lattice parameter changes.

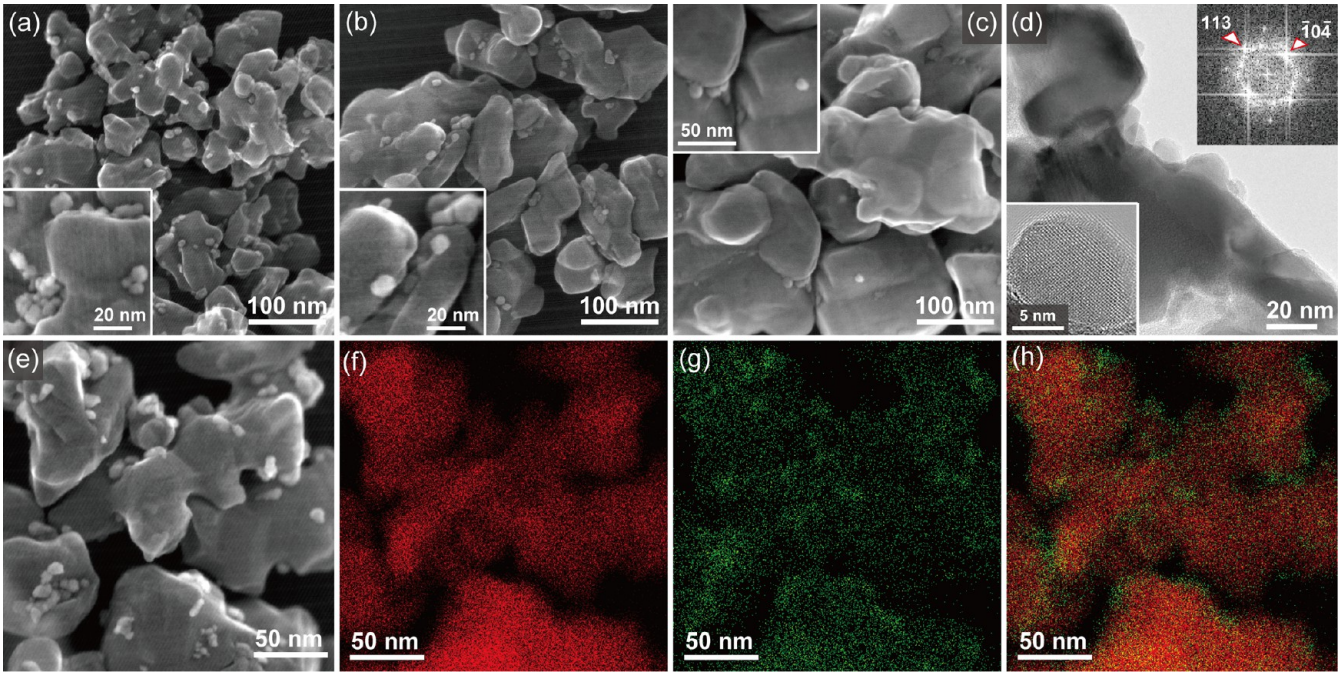

Figure 3. (a)–(c) SE images of samples 700-10, 800-10, and 900-10, respectively. Insets are enlarged images. (d) Bright-field TEM image of sample 700-10. Lower left and upper right insets show an HRTEM image and its corresponding FFT image, respectively. (e) The SE image and elemental mapping images of (f) Fe K and (g) Al K edges for sample 700-10. (h) Merged image of (f) and (g).

formation temperature of $AlFeO_3$ became lower than that in our previous report,[41] presumably owing to the optimization of synthesis conditions. The solid-state reaction in the samples did not reach equilibrium under the heat-treatment conditions, especially because of the short heating time. Therefore, more than two phases coexisted in this system.

The lattice parameters a and c of Al-Hem were determined using silicon as an internal standard, and the solubility limit of Al in hematite at each temperature was determined from the inflection point of composition-dependent curves of these parameters. The lattice parameters decreased with increasing Al molar ratio, and the solubility limit of Al increased with the heating temperature. The solubility limits of Al were determined to be 7.0, 8.4, 10.3, 11.3, and 13.0 mol % at 700, 800, 900, 1000, and 1100 °C, respectively (Figure 2f, dashed line), in close agreement with a previously reported phase diagram Fe_2O_3–Al_2O_3.[41,42] An area of this diagram (Figure 2f, gray area) only showed Al-Hem by XRD even though the loaded Al molar ratio exceeded the solubility limit. Samples prepared under the conditions delimited by this area could

consist of poorly crystalline and/or nanocrystalline Fe−Al oxides.

Microstructure of the Heat-Treated Samples. Heat-treated samples 700-10, 800-10, and 900-10, which belonged in or near the gray area shown in Figure 2f, were subjected to STEM/EDS and HRTEM measurements. SE images acquired by STEM are shown in Figure 3a−c. In all samples, ultrafine particles smaller than 10 nm in diameter were dispersively segregated on large particles exhibiting diameters of 40−100 nm. The number of ultrafine particles decreased with increasing temperature. EDS point analyses of a portion of the large particles provided Al compositions of 6.0, 8.2, and 9.6 mol % for samples 700-10, 800-10, and 900-10, respectively, which are almost consistent with the solubility limits derived from lattice parameters. TEM results for sample 700-10 are shown in Figure 3d. The fast Fourier transform (FFT) pattern of the HRTEM image of an ultrafine particle in sample 700-10 matched the FFT pattern of the corundum structure for an incident beam irradiation from the [$\bar{4}$71] zone axis (insets, Figure 3d), suggesting that ultrafine particles comprise Al-Hem and/or Fe-Cor. Figure 3e−h show the STEM/EDS elemental analysis of sample 700-10. Strong Fe and weak Al signals were detected from large particles, whereas strong Al and weak Fe signals were obtained from ultrafine particles (Figure 3f−h), indicating that large and ultrafine particles are Al-Hem and Fe-Cor, respectively. These results reveal that samples prepared under the conditions delimited by the gray area shown in Figure 2f are nanocomposites of large Al-Hem and ultrafine Fe-Cor particles.

Color Tone of Heat-Treated Samples. In general, hematite color increases in lightness and chroma with decreasing particle size.[14,27,28] Therefore, average particle sizes of heat-treated samples were measured from their SEM images (Figure 4; see Table S2 in the Supporting Information). The

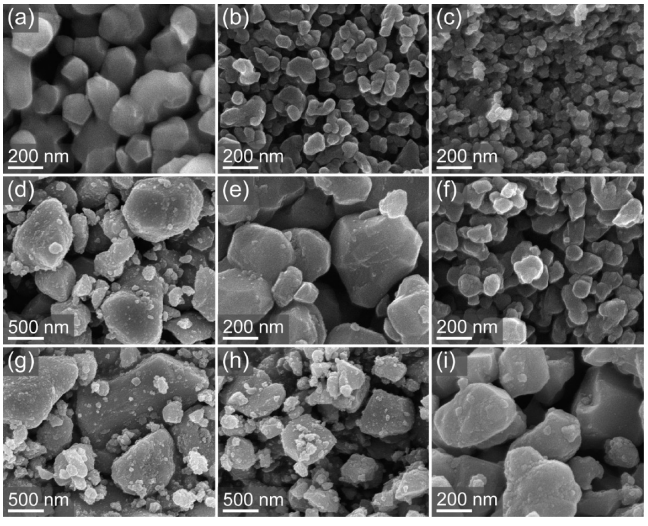

Figure 4. SEM images for samples (a) 700-0, (b) 700-05, (c) 700-10, (d) 900-0, (e) 900-05, (f) 900-10, (g) 1000-0, (h) 1000-05, and (i) 1000-10.

particle size decreased with increasing Al molar ratio and decreasing temperature. This behavior may be reasonably explained through TG-DTA analyses of pyrolytic powders (see Figure S2 in the Supporting Information). For $x \geq 0.05$, pyrolytic samples exhibited broad exothermic peaks corresponding to maghemite-to-hematite transformation temperatures.[43−45] These peaks shifted from ∼610 °C for x = 0.05 to higher temperature with increasing Al molar ratio. A transition temperature of ∼750 °C was obtained at x = 0.30. When the Al molar ratio increased, the maghemite-to-hematite phase transformation shifted to a higher temperature during the heating process, suppressing the growth of the resulting hematite particles. This is consistent with our previous suggestion.[33,41]

Color measurements were conducted on monophasic hematite samples (Figure 2f). The color tone was evaluated using the CIE 1976 $L^*a^*b^*$ color space in which L^* represents lightness and a^* and b^* correspond to chromaticity, i.e., color directions. Positive and negative a^* values indicate reddish and greenish colors, respectively, while positive and negative b^* values represent yellowish and bluish colors, respectively.[26] The color tone of the heat-treated samples systematically changed with the heating temperature (photographs in Figure 5). Figure

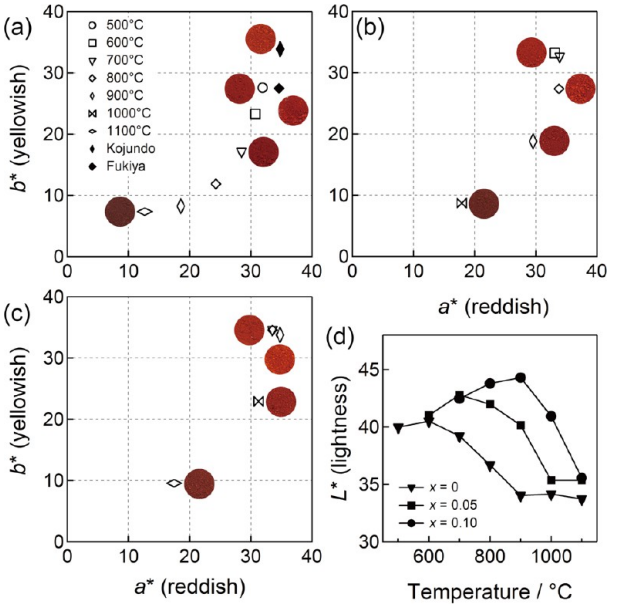

Figure 5. Quantitative analysis of color tone for the heat-treated samples. (a) Plots of a^* and b^* values for Al-free samples heated at 500, 600, 700, 800, 900, and 1100 °C. Commercially available hematite and Fukiya bengala are also shown. (b) Plots of a^* and b^* values for samples 600-05, 700-05, 800-05, 900-05, and 1000-05. (c) Plots of a^* and b^* values for samples 700-10, 800-10, 900-10, 1000-10, and 1100-10. Photographs are shown beside the plots. (d) L^* values of heat-treated samples for x values of 0, 0.05, and 0.10 as a function of temperature. L^*, a^*, and b^* values are summarized in Tables S3 and S4 in the Supporting Information.

5a−c shows the a^* and b^* values of samples heated at different temperatures for x values of 0, 0.05, and 0.10, respectively. Figure 5d shows the change in L^* value as a function of heating temperature for heat-treated samples at different Al molar ratios. Al-free samples heated at 500 °C (lowest temperature, i.e., smallest particle size) exhibited the highest a^* and b^* values. These values decreased when the heating temperature increased (Figure 5a). For x = 0.05, samples heated at 600 and 700 °C showed nearly the same high a^* and b^* values, and these values decreased rapidly above 800 °C (Figure 5b). For x = 0.10, samples heated at 700, 800, and 900 °C showed quasi-similar high a^* and b^* values, and these values drastically decreased above 1000 °C (Figure 5c). The heat-treatment temperature that maximized a^* and b^* values increased with

dx.doi.org/10.1021/am505820b | ACS Appl. Mater. Interfaces 2014, 6, 20282−20289

increasing Al molar ratio. This is nearly consistent with our previous result.[41] L^* values presented local maxima at 600, 700, and 900 °C for x values of 0, 0.05, and 0.10, respectively, and decreased with increasing temperature above these temperatures (Figure 5d). Samples 700-10, 800-10, and 900-10, which displayed the most vivid color (L^* = 42−44, a^* = ∼34, and b^* = ∼34), exhibited almost the same L^*, a^*, and b^* values as commercially available hematite (L^* = 44.6, a^* = 34.8, b^* = 33.9). They also showed higher L^* and b^* values than the model pigment Fukiya bengala (L^* = 41.6, a^* = 34.6, b^* = 27.5).

Two notable points are addressed regarding these color measurements: (i) the change in a^* and b^* values as a function of heat-treatment temperature for Al-containing samples and (ii) the change in L^* value as a function of heat-treatment temperature for Al-free and Al-containing samples. For Al-free samples, a^* and b^* values decreased with increasing temperature (i.e., particle size). In contrast, for x = 0.05, samples heated at 600 and 700 °C showed different particle sizes (∼40 and ∼70 nm, respectively) but almost the same a^* and b^* values. Similarly, for x = 0.10, samples heated at 700, 800, and 900 °C exhibited different particle sizes (∼40, ∼50, and ∼90 nm, respectively) but almost the same a^* and b^* values, suggesting that color does not simply depend on particle size. This trend may result from the Al substitution in the hematite structure, which could enhance lightness and chroma, thereby canceling color fading induced by particle growth. Moreover, for x values of 0, 0.05, and 0.10, the heat-treatment temperature showing the highest L^* value was not the lowest temperature, i.e., the smallest particle size. The highest L^* values were obtained at particle sizes of ∼100, ∼70, and ∼90 nm for x values of 0, 0.05, and 0.10, respectively. A portion of the incident visible light could go through hematite particles instead of being reflected when the particle size is too small (≤100 nm), reducing lightness.

Relation between Color and Al Content. Next, the effect of Al substitution in the hematite structure on hematite color was evaluated. A comparison between the samples exhibiting different Al molar ratios and treated at the same temperature showed that L^*, a^*, and b^* values increased with Al molar ratio for all temperatures. This tendency may partly stem from a difference in particle size. Therefore, the color components of samples displaying the same particle size but different Al molar ratios (i.e., Al substitution values and lattice parameters) were compared. Samples 500-0, 700-5, and 900-10 consisted of 90 nm diameter particles; samples 700-0, 850-5, and 950-10 comprised 160 nm diameter particles; and particles in samples 750-0, 900-5, and 1000-10 were 220 nm in diameter. The lattice parameters of samples presenting the same particle size were calculated, and their Al substitution values were confirmed to be different. L^*, a^*, and b^* values of these samples are shown in Figure 6a. The three sets of samples showed similar trends. L^*, a^*, and b^* values increased with Al molar ratio. The reflectance curves of samples containing 160 nm diameter particles are shown in Figure 6b. The reflectance values at wavelengths exceeding 550 nm increased with Al molar ratio. The reflectance edge shifted toward lower wavelengths with increasing Al molar ratio. These results clearly indicate that Al substitution in the hematite structure intrinsically increases lightness and chroma.

Evaluation of Thermostability by Monitoring Color Change upon Reheating. To study the thermostability, samples 700-10, 800-10, and 900-10 were reheated at 900 °C for 1 h, and their color change was assessed. A commercially available hematite was also reheated as a reference. Variations of L^*, a^*, and b^* values for each sample are shown in Figure 7. For the commercially available hematite, L^*, a^*, and b^* values decreased from 44.6, 34.8, and 33.9 to 32.8, 12.8, and 3.8, respectively (ΔL^* = −11.8, Δa^* = −22.0, and Δb^* = −37.7), showing drastic color fading. On the other hand, the prepared samples exhibited few changes in L^*, a^*, and b^* values, indicating high thermostability. In sample 700-10, the b^* value slightly decreased (Δb^* = −0.3), while L^* and a^* values increased (ΔL^* = 0.9 and Δa^* = 1.7). In sample 800-10, the b^* value also slightly decreased (Δb^* = −0.9), while the a^* value increased (Δa^* = 1.4), but the L^* value remained unchanged (ΔL^* = 0.1). Sample 900-10 exhibited a slight decrease in L^* and b^* values (ΔL^* = −0.9 and Δb^* = −2.2) and an almost unchanged a^* value (Δa^* = 0.5).

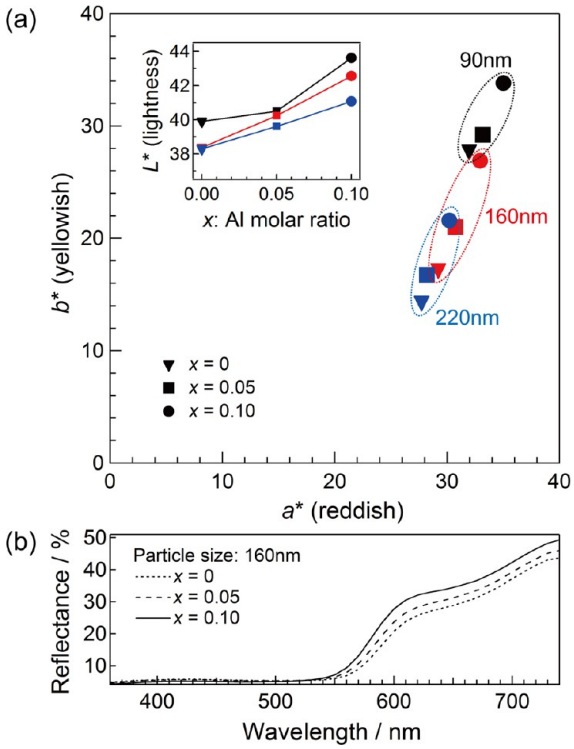

Figure 6. Color comparison between samples exhibiting different Al molar ratios and the same particle size. (a) Plots of a^* and b^* values for the heat-treated samples. Black, red, and blue markers correspond to samples containing 90, 160, and 220 nm diameter particles, respectively. The inset shows L^* values of heat-treated samples as a function of the Al molar ratio. (b) Reflectance curves of samples consisting of 160 nm diameter particles. L^*, a^*, and b^* values are summarized in Table S5 in the Supporting Information.

SE images before and after reheating are shown in Figure 8. In all samples, particle sizes increased drastically and ultrafine Fe-Cor particles almost vanished upon reheating. Despite this particle size growth, the samples' colors remained almost intact. This phenomenon appears to contradict common knowledge: hematite color fades with increasing particle size. Lattice parameters were calculated before and after reheating. For samples of 700-10, 800-10, and 900-10, the lattice parameter a changed from 0.5020, 0.5020, and 0.5016 nm to 0.5017, 0.5017, and 0.5015 nm, respectively, and the lattice parameter c changed from 1.3706, 1.3700, and 1.3685 nm to 1.369, 1.3688, and 1.3682 nm, respectively. These shortened lattice

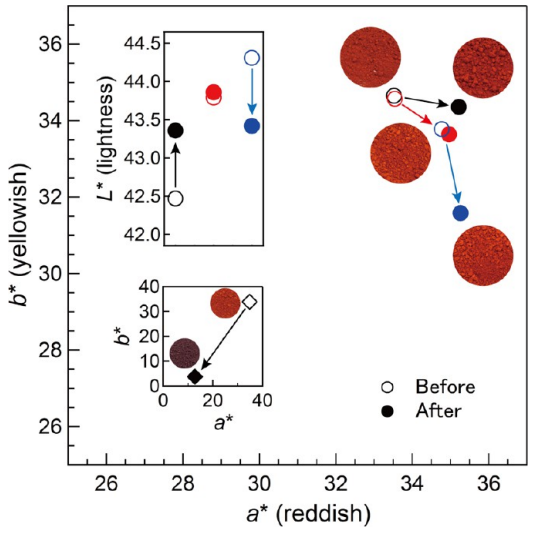

Figure 7. Color variation of samples 700-10, 800-10, and 900-10 after reheating at 900 °C for 1 h in air. Open and closed symbols represent before and after reheating at 900 °C, respectively. Black, red, and blue circles correspond to samples 700-10, 800-10, and 900-10, respectively. The lower inset shows the color variation of commercially available hematite. The upper inset shows the change in L^* for heat-treated samples. L^*, a^*, and b^* values are summarized in Table S6 in the Supporting Information.

parameters and the vanishing ultrafine particles suggest that ultrafine Fe-Cor particles react with large Al-Hem particles upon reheating, promoting additional Al substitution in hematite structures. These results clearly demonstrate why samples 700-10, 800-10, and 900-10 display excellent thermostability. Color fading in hematite resulting from particle growth should be canceled by the effect of Al substitution, which enhances lightness and chroma in hematite. The mechanism explaining the excellent thermostability of these Fukiya bengala-inspired materials differs significantly from that of well-known inclusion pigments.[18−25] This insight will open new doors in the creation of pigments with vivid color and excellent stability as well as novel functional nanocomposite materials. The chemical stability in the molten glazes is extremely important, and it will be studied in the near future by our group.

CONCLUSIONS

To create powder pigments displaying a vivid yellowish-red color and high thermostability, Al-substituted hematite samples inspired by the traditional Fukiya bengala were synthesized and their microstructure, color tone, and thermostability were investigated in detail. Color measurements revealed that the monophasic hematite samples containing 10 mol % Al and heat-treated at 700, 800, and 900 °C displayed high L^*, a^*, and b^* values. XRD, HRTEM, and STEM/EDS measurements showed that a part of the loaded Al was segregated into ultrafine Fe-substituted corundum particles. A comparison between samples presenting the same particle size and different Al molar ratios demonstrated that L^*, a^*, and b^* values increased with the Al molar ratio, revealing that Al substitution in the hematite structure intrinsically enhances lightness and chroma in hematite color. Samples containing 10 mol % Al and heat-treated at 700, 800, and 900 °C mostly retained their color upon heating at a high temperature of 900 °C, indicating high thermostability. These composite materials, which consist of Al-substituted hematite particles and Fe-substituted corundum ultrafine particles, are expected to serve as functional materials in various fields, such as pigments for porcelain bodies, cosmetics, and nanotechnology.

ASSOCIATED CONTENT

Supporting Information

Sample preparation conditions, samples' particle size, the result of DTA measurements, and L^*, a^*, and b^* values are described in the Supporting Information. This material is available free of charge via the Internet at http://pubs.acs.org.

AUTHOR INFORMATION

Corresponding Author

*E-mail: hideki-h@cc.okayama-u.ac.jp (H.H.).

Notes

The authors declare no competing financial interest.

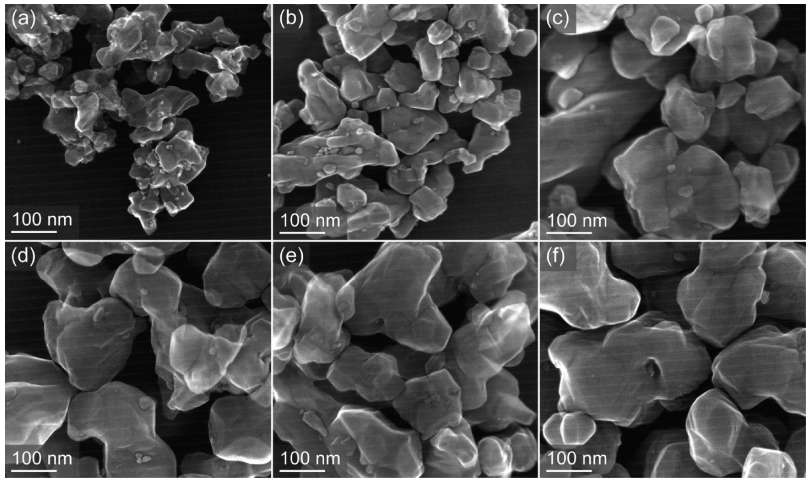

Figure 8. SE images before reheating samples (a) 700-10, (b) 800-10, and (c) 900-10. SE images after reheating samples (d) 700-10, (e) 800-10, and (f) 900-10.

■ ACKNOWLEDGMENTS

The authors thank Dr. Yasunori Ikeda and Dr. Ryu Murakami for their helpful discussions.

■ REFERENCES

(1) Wagloehner, S.; Reichert, D.; Leon-Sorzano, D.; Balle, P.; Geiger, B.; Kureti, S. Kinetic Modeling of the Oxidation of CO on Fe_2O_3 Catalyst in Excess of O_2. *J. Catal.* **2008**, *260*, 305−314.

(2) Huo, L.; Li, W.; Lu, L.; Cui, H.; Xi, S.; Wang, J.; Zhao, B.; Shen, Y.; Lu, Z. Preparation, Structure, and Properties of Three-Dimensional Ordered α-Fe_2O_3 Nanoparticulate Film. *Chem. Mater.* **2000**, *12*, 790−794.

(3) Chen, J.; Xu, L.; Li, W.; Gou, X. α-Fe_2O_3 Nanotubes in Gas Sensor and Lithium-Ion Battery Applications. *Adv. Mater.* **2005**, *17*, 582−586.

(4) Cabana, J.; Monconduit, L.; Larcher, D.; Palacin, M. R. Beyond Intercalation-Based Li-Iion Batteries: The State of the Art and Challenges of Electrode Materials Reacting through Conversion Reactions. *Adv. Mater.* **2010**, *22*, E170−E192.

(5) Ji, L.; Lin, Z.; Alcoutlabi, M.; Zhang, X. Recent Developments in Nanostructured Anode Materials for Rechargeable Lithium-Ion Batteries. *Energy Environ. Sci.* **2011**, *4*, 2682−2699.

(6) Björkstén, U.; Moser, J.; Grätzel, M. Photoelectrochemical Studies on Nanocrystalline Hematite Films. *Chem. Mater.* **1994**, *6*, 858−863.

(7) Seki, M.; Yamahara, H.; Tabata, H. Enhanced Photocurrent in Rh-Substituted α-Fe_2O_3 Thin Films Grown by Pulsed Laser Deposition. *Appl. Phys. Express* **2012**, *5*, 115801.

(8) Yang, T.-Y.; Kang, H.-Y.; Jin, K.; Park, S.; Lee, J.-H.; Sim, U.; Jeong, H.-Y.; Joo, Y.-C.; Nam, K. T. An Iron Oxide Photoanode with Hierarchical Nanostructure for Efficient Water Oxidation. *J. Mater. Chem. A* **2014**, *2*, 2297−2305.

(9) Matijevic, E.; Scheiner, P. Ferric Hydrous Oxide Sols: III. Preparation of Uniform Particles by Hydrolysis of Fe (III)-Chloride, -Nitrate, and -Perchlorate Solutions. *J. Colloid Interface Sci.* **1978**, *63*, 509−524.

(10) Sugimoto, T.; Wang, Y.; Itoh, H.; Muramatsu, A. Systematic Control of Size, Shape and Internal Structure of Monodisperse α-Fe_2O_3 Particles. *Colloids Surf., A* **1998**, *134*, 265−279.

(11) Han, L.-H.; Liu, H.; Wei, Y. In Situ Synthesis of Hematite Nanoparticles Using a Low-Temperature Microemulsion Method. *Powder Technol.* **2011**, *207*, 42−46.

(12) Horiishi, N. A Historical Survey of Bengala in View of Art and Science. *J. Jpn. Soc. Powder Powder Metall.* **2002**, *49* (12), 1121−1127.

(13) Buxbaum, G.; Pfaff, G. *Industrial Inorganic Pigments*, 3rd ed.; Wiley-VHC Verlag GmbH & Co. KGaA: Weinheim, 2005.

(14) Cornell, R. M.; Schwertmann, U. *The Iron Oxides: Structure, Properties, Reactions, Occurrences, and Uses*, 2nd ed.; Wiley-VHC Verlag GmbH & Co. KGaA: Weinheim, 2004.

(15) Takada, T. Studies on Iron Red Glazes. *J. Jpn. Soc. Powder Powder Metall.* **1958**, *4*, 169−186.

(16) Katsuki, H.; Komarneni, S. Microwave-Hydrothermal Synthesis of Monodispersed Nanophase α-Fe_2O_3. *J. Am. Ceram. Soc.* **2001**, *84*, 2313−2317.

(17) Katsuki, H.; Komarneni, S. Role of α-Fe_2O_3 Morphology on the Color of Red Pigment for Porcelain. *J. Am. Ceram. Soc.* **2003**, *86*, 183−185.

(18) Bondioli, F.; Ferrari, A. M.; Leonelli, C.; Manfredini, T. Synthesis of Fe_2O_3/Silica Red Inorganic Inclusion Pigments for Ceramic Applications. *Mater. Res. Bull.* **1998**, *33*, 723−729.

(19) Hosseini-Zori, M.; Bondioli, F.; Manfredini, T.; Taherinassaj, E. Effect of Synthesis Parameters on a Hematite−Silica Red Pigment Obtained Using a Coprecipitation Route. *Dyes Pigm.* **2008**, *77*, 53−58.

(20) Hosseini-Zori, M.; Taheri-Nassaj, E. Nano Encapsulation of Hematite Into Silica Matrix as a Red Inclusion Ceramic Pigment. *J. Alloys Compd.* **2012**, *510*, 83−86.

(21) Zhang, Y.; Rao, P.; Lü, M.; Zeng, D.; Wu, J. Synthesis and Color Evolution of Silica-Coated Hematite Nanoparticles. *J. Am. Ceram. Soc.* **2009**, *92*, 1877−1880.

(22) Zhao, F.; Li, W.; Luo, H. Sol−Gel Modified Method for Obtention of Gray and Pink Ceramic Pigments in Zircon Matrix. *J. Sol-Gel Sci. Technol.* **2009**, *49*, 247−252.

(23) Zhao, F.; Gao, Y.; Luo, H. Reactive Formation of Zircon Inclusion Pigments by Deposition and Subsequent Annealing of a Zirconia and Silica Double Shell. *Langmuir* **2009**, *25*, 13295−13297.

(24) Kim, Y. J.; Pee, J. H.; Chang, J. H.; Choi, K.; Kim, K. J.; Jung, D. Y. Silica Effect on Coloration of Hematite Nanoparticles for Red Pigments. *Chem. Lett.* **2009**, *38*, 842−843.

(25) Yu, R.; Kim, Y.; Pee, J. H.; Kim, K. J.; Kim, W. Thermal Behavior and Coloration Study of Silica-Coated α-Fe_2O_3 and β-FeOOH Nanoparticles. *J. Nanosci. Nanotechnol.* **2011**, *11*, 6283−6286.

(26) OhnoY.CIE Fundamentals for Color Measurements. In *Proceedings of the IS&T NIP16 Conference*, Vancouver, Canada, Oct 16−20, 2000.

(27) Takada, T. On the Effects of Particle Size and Shape on the Colour of Ferric Oxide Powders. *J. Jpn. Soc. Powder Powder Metall.* **1958**, *4*, 160−168.

(28) Kusano, Y.; Fukuhara, M.; Takada, J.; Doi, A.; Ikeda, Y.; Takano, M. Science in the Art of the Master Bizen Potter. *Acc. Chem. Res.* **2010**, *43*, 906−915.

(29) Schabbach, L. M.; Bondioli, F.; Ferrari, A. M.; Manfredini, T.; Petter, C. O.; Fredel, M. C. Color in Ceramic Glazes: Analysis of Pigment and Opacifier Grain Size Distribution Effect by Spectrophotometer. *J. Eur. Ceram. Soc.* **2008**, *28*, 1777−1781.

(30) Earl, D. A.; Clark, D. E. Effects of Glass Frit Oxides on Crystallization and Zircon Pigment Dissolution in Whiteware Coatings. *J. Am. Ceram. Soc.* **2000**, *83*, 2170−2176.

(31) Bolnski, R. P. Higher-Chroma Zircon Colors for Glaze Applications. *Ceram. Eng. Sci. Proc.* **1994**, *15*, 266−280.

(32) Nagao, T. *Fukiya no Hanashi ~Dentou to Bunka no Machi Dai San Syu~*; The Sanyo Shimbun: Okayama, Japan, 1976.

(33) Asaoka, H.; Kusano, Y.; Nakanishi, M.; Fujii, T.; Takada, J. Characterization and Reproduction of "Fukiya Bengara," Noble Red Color Pigment, by Fe_2O_3-Al_2O_3 System. *J. Jpn. Soc. Powder Powder Metall.* **2003**, *50*, 1062−1067.

(34) Kondo, Y.; Yoshida, A. *Zusetsu Okayama-ken no Rekishi*; Kawade Shobo Shinsha: Tokyo, 1990.

(35) Kajihara, S.; Hidaka, M.; Wijesundera, R. P.; Kumara, L. S. R.; Koga, M.; Kobayashi, S.; Tsuru, T.; Koga, K.; Shimomura, K.; Choi, J.-Y.; Sung, N. E.; Park, Y. J. Correlation between the Izumiyama Porcelain Ceramics and the Red-Overglaze Enamels of the Kakiemon-Style Porcelains. *Ceram. Int.* **2008**, *34*, 1681−1689.

(36) Hidaka, M.; Horiuchi, H.; Ohashi, K.; Wijesundera, R.; Kumara, L.; Choi, J. Y.; Park, Y. J. Structural Properties of the Red-Color Overglazes on the Kakiemon-style Porcelains Produced in the Later 17th Century by Means of X-rayDiffraction (I). *Cerâmica* **2009**, *55*, 120−127.

(37) *Earth and Fire: The Historical Development of Kyushu Ceramics. The The Kyushu Ceramic Museum Guide Book*; Sanko Co., Ltd: Saga, Japan, 1996.

(38) *Commemorative Exhibition of the Shibata Donation: Shibata Collection VIII: The Splendor of Ko-Imari*; The Kyushu Ceramic Museum: Saga, Japan, 2002.

(39) Schiffer, N. N. *Imari Satsuma and Other Japanese Export Ceramics*, 2nd ed.; Schiffer Publishing Ltd.: Atglen, PA, 2000.

(40) Shimura, G. *The Story of Imari: The Symbols and Mysteries of Antique Japanese Porcelain*; Ten Speed Press: Berkeley, CA, 2008.

(41) Asaoka, H.; Nakanishi, M.; Fujii, T.; Takada, J. Preparation and Characterization of Al-Substituted Hematite and Their Tone Color. In *Ninth Internal Conference on Ferrites ICF 9: Proceeedings of the International Conference of Ferrites (ICF-9)*, San Fransisco, CA, 2004; Wiley-Blackwell: Hoboken, NJ, 2005; pp 69−74.

(42) Barry, T. I.; Dinsdale, A. T.; Gisby, J. A. The Compound Energy Model for Ionic Solutions with Applications to Solid Oxides. *J. Phase Equilib.* **1992**, *13*, 459−475.

(43) Sidhu, P. S. Transformation of Trace Element-Substituted Maghemite to Hematite. *Clays Clay Miner.* **1988**, *36*, 31−38.
(44) Ye, X.; Lin, D.; Jiao, Z.; Zhang, L. The Thermal Stability of Nanocrystalline Maghemite Fe_2O_3. *J. Phys. D: Appl. Phys.* **1998**, *31*, 2739−2744.
(45) Chen, D.; Xu, R. Hydrothermal Synthesis and Characterization of Nanocrystalline γ-Fe_2O_3 Particles. *J. Solid State Chem.* **1998**, *137*, 185−190.